Defense Technical Information Center Compilation Part Notice

ADP012603

TITLE: Multi-Color Quantum Well Infrared Photodetectors for Mid-, Long-, and Very Long- Wavelength Infrared Applications

DISTRIBUTION: Approved for public release, distribution unlimited

This paper is part of the following report:

TITLE: Progress in Semiconductor Materials for Optoelectronic Applications Symposium held in Boston, Massachusetts on November 26-29, 2001.

To order the complete compilation report, use: ADA405047

The following component part numbers comprise the compilation report:
ADP012585 thru ADP012685

Mat. Res. Soc. Symp. Proc. Vol. 692 © 2002 Materials Research Society

Multi-Color Quantum Well Infrared Photodetectors for Mid-, Long-, and Very Long- Wavelength Infrared Applications (invited)

Sheng S. Li
Department of Electrical and Computer Engineering
University of Florida, Gainesville, FL 32611
Email address: shengli@eng.ufl.edu

ABSTRACT

Quantum well infrared photodetectors (QWIPs) have been widely investigated for the 3-5 μm mid-wavelength infrared (MWIR) and 8-12 μm long-wavelength infrared (LWIR) atmospheric spectral windows as well as very long wavelength infrared (VLWIR: λ_c > 14 μm) detection in the past decade. The mature III-V compound semiconductor growth technology and the design flexibility of device structures have led to the rapid development of various QWIP structures for infrared focal plane arrays (FPAs) applications. In addition to the single-color QWIP with narrow bandwidth, the multi-color QWIP required for advanced IR sensing and imaging applications have also been emerged in recent years. Using band gap engineering approach, the multi-color (2, 3, and 4- color) QWIPs using multi-stack quantum wells with different well width and depth and voltage-tunable triple- coupled quantum well (TCQW) structure for detection in the MWIR, LWIR, and VLWIR bands have been demonstrated. In this paper, the design, fabrication, and characterization of a voltage-tunable 2-stack 3-color QWIP for MW/LW/LW IR detection and a 3-stack 3-color QWIP for detection in the water, ozone, and CO_2 atmospheric blocking bands are depicted.

1. INTRODUCTION

Recent advances in III-V semiconductor epitaxial layer growth techniques such as molecular beam epitaxy (MBE) [1] and metalorganic chemical vapor deposition (MOCVD) have made it possible to grow a wide variety of novel semiconductor hetero-structures. Significant progress has been made in quantum wells and superlattice optoelectronic devices using these growth techniques. The quantum well is formed by using an ultra thin layer of narrow band gap semiconductor (e.g., GaAs) sandwiched between two thin wider band gap semiconductor (e.g., AlGaAs) barrier layers. The motion of the carriers perpendicular to the layers becomes quantized so that localized two-dimensional subbands of quantized states are formed inside the quantum well. [2]

Early proposals of using optical intersubband transitions in quantum wells for IR detection were made by Chang et al. [3], Esaki, Tsu, and Sakaki[4-5], and Coon and Karunasiri [6]. The intersubband absorption in GaAs quantum wells was first observed by West and Eglash [7] and followed by Harwit and Harris [8]. Levine et al. [9] demonstrated the first GaAs QWIP in 1987. Since then, QWIPs based on the bound-to-bound (B-B), bound-to-continuum (B-C) [10], and bound-to-miniband (B-M) [11]transitions have been widely investigated for the 3 to 5 μm mid-wavelength infrared

(MWIR) and 8 to 14 μm long-wavelength infrared (LWIR) detection [12-13]. Additionally, there is a considerable interest in the development of multi-stack and voltage- tunable asymmetrical coupled quantum well structures for multi-color focal plane array (FPA) applications in the MWIR and LWIR atmospheric spectral windows. [14]

One major difference between the QWIP and other IR detectors is that QWIPs use intersubband transitions either in the conduction band (n-type) or in the valence band (p-type) to detect IR radiation. The basic intersubband transition schemes for n-type QWIPs include (a) bound-to-bound (B-B), (b) bound-to-continuum (B-C), (c) bound-to-miniband (B-M), and (d) bound-to-quasi-bound (BQB) transitions. By using different well widths and barrier heights, the detection wavelengths of QWIPs can be tuned from 3 to 20 μm and beyond. Depending on where the upper excited states are located and the barrier layer structure, the intersubband transitions in a QWIP can be based on the B-B state, B-M state, BQB state, and the B-C state transitions. Among the various types of QWIPs reported, the GaAs/AlGaAs QWIP structures using the B-C and B-M transitions are the most widely used material systems and structures for the fabrication of large format FPAs for MWIR and LWIR imaging applications. Multi-color QWIPs using the multi- stack and voltage-tunable asymmetrical coupled quantum well structures such as the triple-coupled (TC-) QWIP have received considerable interest in recent years. [14-18] The multi-stack structure is usually employed to obtain multi-color detection in the MWIR and LWIR atmospheric spectral windows. Using quantum confined Stark effect, the voltage tunable TC- QWIP has also been reported for multi-color detection. [14,16]

Section 2 presents a voltage-tunable 2-stack 3-color QWIP for the MW/LW/LW IR detection using an InGaAs/AlGaAs B-C QWIP for the MWIR stack and an InGaAs/AlGaAs/GaAs TC- QWIP for the LWIR stack. A 3-stack 3-color QWIP using the graded barrier structure for detection in the water (MWIR), ozone (LWIR), and the CO_2 (VLWIR) atmospheric blocking bands is depicted in section 3. Conclusions are given in section 4.

2. A 2-STACK 3-COLOR QWIP FOR MWIR/LWIR DETECTION

A 2-stack 3-color QWIP structure used in this study was grown on a semi-insulating (SI) GaAs substrate by using the molecular beam epitaxy (MBE) technique. The bottom stack is an InGaAs/AlGaAs B-C QWIP grown on the semi-insulating (SI) GaAs substrate for MWIR detection. This MWIR QWIP consists of 3 periods of a 4.3 nm $In_{0.3}Ga_{0.7}As$ quantum well Si-doped to $N_d = 2.5\times10^{18}$ cm^{-3} and an undoped 30 nm $Al_{0.3}Ga_{0.7}As$ barrier. The ohmic contact layers (Si-doped to $N_d = 2\times10^{18}$ cm^{-3}) were grown on the top and bottom of the MWIR stack. The top stack is a two- color TC- QWIP, which was grown on top of the MWIR stack for LWIR detection. The basic structure of the TC-QWIP is composed of 5 periods of TCQW separated by two thin (20 Å) $Al_{0.08}Ga_{0.92}As$ barrier layers. The TCQW is formed by a 65 Å Si-doped (7×10^{17} cm^{-3}) $In_{0.18}Ga_{0.82}As$ deep well and two 60 Å undoped $In_{0.05}Ga_{0.95}As$ shallow wells. In this structure, the well width was designed to create three subbands (i.e., E_1, E_2, and E_3 states) within the quantum wells with dominant transitions from the E_1 to E_3 and E_1 to E_c states, with detection peak wavelengths longer than previously reported values.[17] For ohmic contacts, two heavily

doped ($N_d = 2\times10^{18}$ cm^{-3}) GaAs contact layers were grown on the top and bottom of the active TCQW absorber layers. To reduce the tunneling injection current from contacts to the quantum wells, a 100 nm thick undoped GaAs spacer layer was also grown between the active TCQW absorber layers and the top/bottom contact layers.

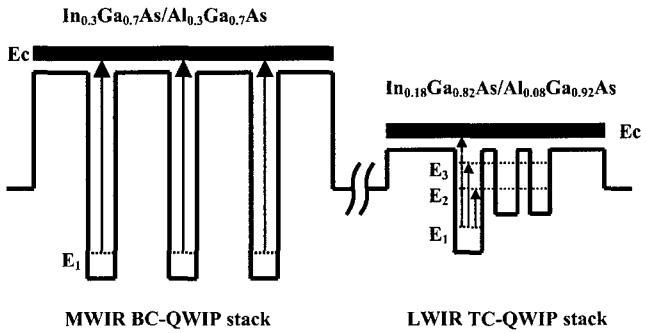

Figure 1 The schematic energy band diagram for a 2-stack 3-color QWIP

Figure 1 shows the schematic conduction band diagrams and the intersubband transition scheme for this 2-stack MWIR BC-QWIP and LWIR TC-QWIP. For the TC-QWIP, due to the strong coupling effect of the three asymmetrical QWs and two thin AlGaAs barriers, the bound states in the shallow wells and the first and second excited states in the deep well are coupled to form the second and third bound states (i.e., E_2 and E_3 states) inside the quantum wells. In this TC-QWIP stack, we observed two detection peaks in the LWIR band under negative bias condition. The first peak, which corresponds to the E_1-E_C bound-to-continuum (BC) transition, was observed at 10 μm and shifted to 9.2 μm when the applied bias varied from –1.2 V to –1.9 V. When the bias voltage was increased above –1.4 V, a second peak appeared around 12 μm, which corresponds to the bound-to-bound (BB) states transition between the E_1 and E_3 states as shown in Figure 1. By increasing the bias voltage from –1.5 V to –1.9 V we also observed the wavelength shifting from 12.2 μm to 12 μm for the second peak. As for the MWIR BC-QWIP the peak detection wavelength corresponding to the E_1 to E_C states transition is at 5.1 μm.

Figure 2 (a) and (b) show the dark current density-voltage (J-V) characteristics for this QWIP device measured at different temperatures along with the 300K- background window current measured with an 180° field of view (FOV) at 20K. As expected from the asymmetrical quantum well structure, the dark current curves of the TC-QWIP stack are highly asymmetrical under positive and negative bias conditions. This asymmetrical J-V characteristic is attributed to the difference in the effective barrier height experienced by the electrons under positive and negative bias conditions. The MWIR QWIP stack is under background limited performance (BLIP) for $-0.95V < V_b < 0.9V$ at T = 77 K, and the BLIP temperature is at T = 90 K for $-0.5V < V_b < 0.4V$.

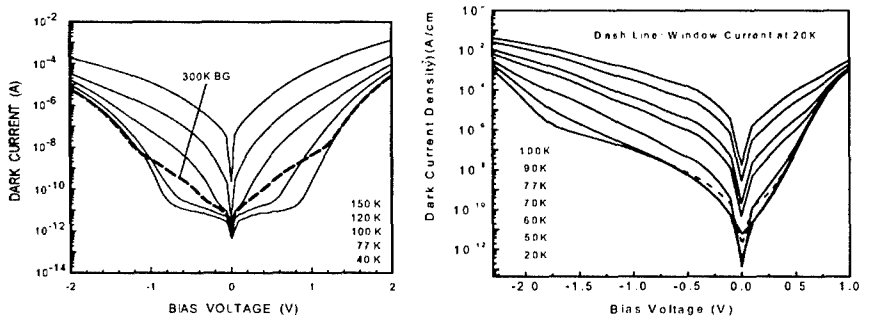

(a) Bottom stack (B-C QWIP) (b) Top stack (TC-QWIP)

Figure 2 Dark I-V characteristics for the 2-stack 3-color QWIP.

Figure 3 (a), (b), (c), and (d) show the spectral responsivity of the MWIR QWIP stack measured at different bias voltages and temperatures. The photoresponse was due to the B-C states transition for this MWIR QWIP stack. At T = 77 K, the peak responsivities under negative biases were found to increase with the bias voltage up to –1.3V and the

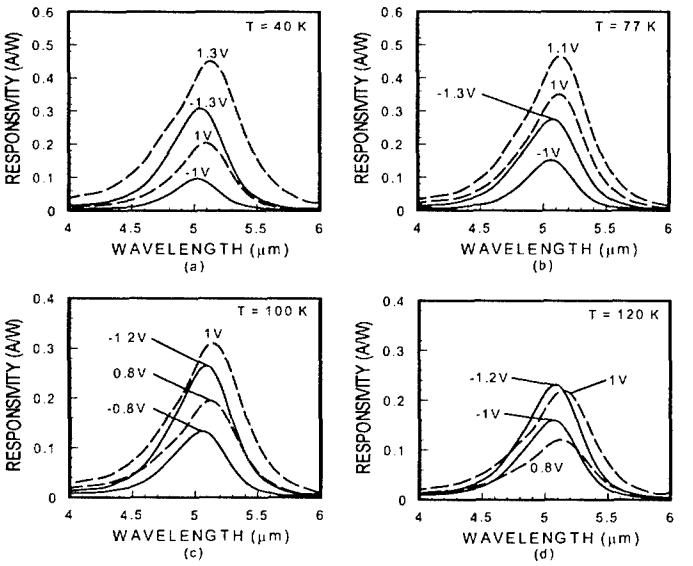

Figure 3 Spectral responsivity of the MWIR QWIP stack measured at T = 40, 77, 100, and 120 K for the 2-stack 3-color QWIP.

maximum responsivity was 0.27 A/W at λ_p = 5.1 μm and V_b = –1.3V, and the peak responsivity was 0.46 A/W at λ_p = 5.1 μm, V_b = 1.1V and T = 77 K. The peak wavelength at λ_p = 5.1 μm was found to be nearly independent of the bias voltage and temperature.

Figure 4 shows the spectral responsivity for the LWIR TC-QWIP stack under negative biases and at T = 40 K. The peak responsivity due to the E_1-E_3 state transition under negative bias was 1.96 A/W at λ_p = 12 μm and V_b = –1.9 V. Under the positive bias condition, the peak responsivity due to the E_1-E_C transition was found to be 0.11A/W at λ_p = 9.5 μm and V_b = 0.6 V. The relatively low responsivity observed under positive bias was attributed to the very large dark current, which makes the device easily saturated with the dark current even under very small positive bias condition.

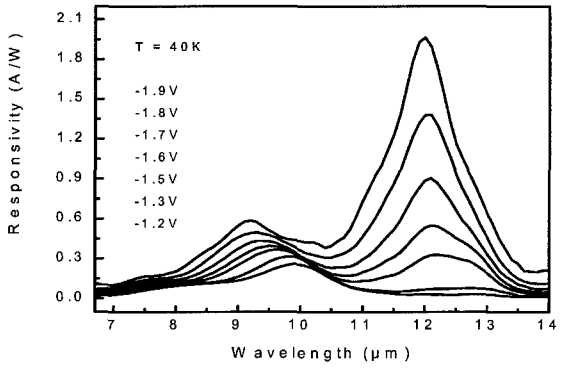

Figure 4 Spectral responsivity of the LWIR TC-QWIP stack for the 2-stack 3-color QWIP.

Figure 5 (a) and (b) show the quantum confined Stark shift of the peak detection wavelength versus applied bias for the TC-QWIP for the E_1-E_C and the E_1-E_3 transitions, which exhibit a linear dependence of the peak wavelength on the applied bias voltage. The wavelength tunability by the applied bias was achieved in the range from 9.2 μm to 10 μm and 12 μm to 12.2 μm for the E_1-E_C and E_1-E_3 transitions, respectively. The detectivity was calculated from the measured responsivity and dark current. The peak detectivity, D^*, for the TC-QWIP can be obtained by using the calculated noise gain from the zero bias dark current value and the measured responsivity, which was found to be $D^* = 1.59 \times 10^{10}$ cm-Hz$^{1/2}$/W at λ_p = 12 μm, V_b = –1.7 V, and T = 20 K.

A voltage tunable 2-stack 3-color QWIP using the InGaAs/AlGaAs material systems for the MWIR stack and a voltage-tunable TC-QWIP using $In_{0.18}Ga_{0.82}As/Al_{0.08}Ga_{0.92}As/In_{0.05}Ga_{0.95}As$ material systems for LW/LW two-color detection has been demonstrated in this section. A linear dependence of the two peak wavelengths with applied bias for the TC-QWIP stack was observed in this device. By varying the bias voltages from –1.2 V to

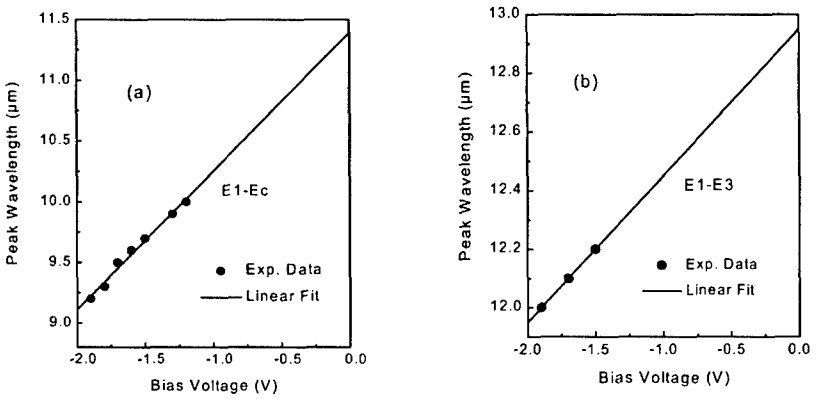

Figure 5 The peak detection wavelength vs. bias voltage for the E_1-E_c and E_1-E_3 state transition peaks for the LWIR TC-QWIP stack.

–1.9 V and –1.5 V to –1.9 V, the wavelengths of two detection peaks shift from 10 μm to 9.2 μm and 12.2 μm to 12 μm, respectively. The highest peak responsivity under negative bias was found to be 1.96 A/W at λ_p = 12 μm, V_b = –1.9 V, and T = 40K. The maximum detectivity for the λ_p = 12 μm peak was found to be $D^* = 1.59\times10^{10}$ cm-$Hz^{1/2}$/W at V_b = –1.7 V and T = 20 K. As for the MWIR QWIP stack excellent responsivity for the 5.1 μm peak was obtained up to 120 K. This 2-stack 3- color QWIP can be used for detection in the MW/LW/LW IR spectral windows for 3-color FPAs applications.

3. A 3-STACK 3-COLOR QWIP FOR H_2O, CO, AND CO_2 BANDS DETECTION

Although QWIPs have been widely investigated for detection in the 3~5 μm MWIR, and 8~14 μm LWIR atmospheric spectral windows in the past decade, however, none of the reported multi-color QWIPs have been designed specifically for detection in the atmospheric blocking bands. There are three blocking bands in the MWIR to VLWIR regions that can be used for practical IR detection. These are the water band (5.5- 7.5 μm), the ozone (O_3) band (9.4- 9.9 μm), and the CO_2 band (14- 16 μm), and none of these bands blocks the earthshine completely at exo-atmosphere. In a 3- color temperature estimation with earthshine in the exo-atmosphere, the accuracy of the earthshine ratio terms is maximized if one of the detector colors is chosen in a band where the earth atmosphere partially blocks the earthshine. [18] Therefore the sensitivity of a QWIP device with one detection wavelength in the above blocking bands will be improved if the detector is used in exo-atmospheric interceptors, space-based surveillance sensors, or satellite mapping. This technology can be used for multi-color focal plane arrays (FPAs), which is an essential application for QWIPs. In this section, we present a specially designed 3- stack, 3- color QWIP with detection wavebands in the MWIR,

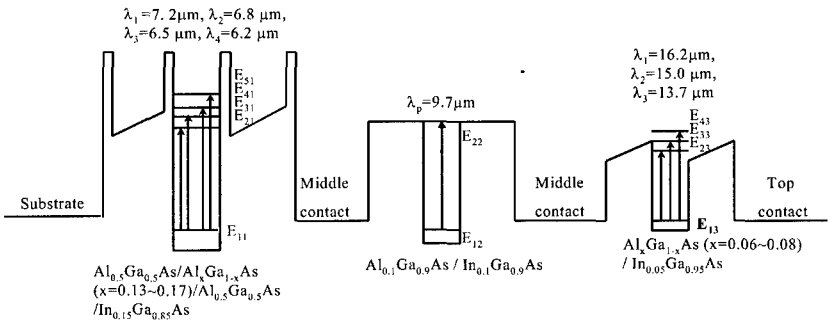

Figure 6 The schematic conduction band diagram of the 3-stack 3-color QWIP for the MW/LW/VLWIR detection covering the water, ozone, and CO_2 blocking bands.

LWIR, and VLWIR spectral ranges that cover the above three atmospheric blocking bands.

Figure 6 shows the schematic conduction band diagram and intersubband transition schemes of a 3-stack 3-color QWIP for the MW/LW/VLW IR detection. The bottom stack is designed to detect the infrared radiation with wavelengths covering the water blocking band. This stack consists of 5 periods of 500Å $Al_xGa_{1-x}As$ barrier and 64 Å $In_{0.15}Ga_{0.85}As$ well doped to $N_d=2\times10^{18}$ cm^{-3}. The 500Å $Al_xGa_{1-x}As$ barrier is composed of 460 Å $Al_xGa_{1-x}As$ graded barrier with x varied from 0.13 on the substrate side to 0.17 and two 20 Å $Al_{0.5}Ga_{0.5}As$ tunneling barriers grown on both sides of the graded barrier. The middle stack is designed to detect the wavelengths covering the ozone- blocking band. This stack was grown using 10 periods of 500Å $Al_{0.1}Ga_{0.9}As$ barrier and 63 Å $In_{0.1}Ga_{0.9}As$ well doped to $N_d=8\times10^{17}$ cm^{-3}. The detection wavelengths for the top stack cover the CO_2 blocking band, and this stack was grown with 20 periods of 500Å $Al_xGa_{1-x}As$ barrier and 60 Å $In_{0.05}Ga_{0.95}As$ well doped to $N_d=5\times10^{17}$ cm^{-3}. The $Al_xGa_{1-x}As$ barrier was graded from x=0.06 on the substrate side to 0.08. The three stacks are separated by a 0.5 μm and 0.6 μm thick of highly doped intermediate contact layers, and the entire stacks were sandwiched between the 0.3 μm top - and the 0.7 μm bottom- contact layers. All the contact layers were doped with silicon impurity to $N_d= 2\times10^{18}$ cm^{-3} to attain low contact resistance.

The multi-layer transfer matrix method (TMM) was used to calculate the peak detection wavelengths for this 3- stack 3-color QWIP.[19] The calculated peak detection wavelength for the bottom stack is 6.5 μm, which is centered at the water- blocking band. As shown in Figure 6, the IR detection is based on the intersubband transition from the localized ground state (E_{11}) to the bound states (E_{21}, E_{31}) and the quasi-continuum states (E_{41}, E_{51}), and the peak wavelength corresponds to the $E_{11}\rightarrow E_{41}$ transition since E_{41} is the nearest energy state to the top of the graded barrier (i.e., $Al_xGa_{1-x}As$ with x = 0.17) where

the excited state is confined inside the quantum well with the highest electron escape probability.[20] The thin $Al_{0.5}Ga_{0.5}As$ double barriers are used to increase the barrier height which gives a larger energy spacing between the ground state and the excited states for the MWIR stack. The main benefit of the graded barriers is that it creates multiple excited states, which result in a broader detection bandwidth as compared to the regular rectangular QWIP used in the MWIR band.

The calculated peak wavelength for the LWIR stack is 9.7μm, which is centered at the ozone- blocking band. The IR detection is based on the intersubband transition from the ground E_{12} to the quasi-bound E_{22} states. To prevent the overlapping of IR detection wavelengths with the bottom stack (MWIR), we employ the ground to quasi-bound state intersubband transition, which has a narrower bandwidth than the ground-continuum state transition. In addition, E_{22} is in resonance with the top of the barrier to achieve maximum responsivity.

The calculated peak detection wavelength for the top stack is 15 μm. The dominant intersubband transitions are from the ground state E_{13} to the bound states E_{23}, quasi-bound state E_{33}, and to the continuum state E_{43}. The peak responsivity is expected from the transition of the E_{13} to E_{33} states. The major concern with a VLWIR QWIP is the high dark current caused by the thermionic emission at the desired operating temperature due to its low energy barrier. Using graded barriers can reduce the dark current under negative bias conditions as compared to the rectangular barriers.

$In_xGa_{1-x}As$ quantum wells were used in all three QWIP stacks to enhance the intersubband absorption due to the smaller electron effective mass in this material system than that of GaAs. This in turn will increase the detection sensitivity of optical signals that are partially blocked by the water, ozone, and CO_2 bands in the atmosphere. The number of QWs, barrier widths and doping densities are chosen so that reasonable bias voltage distribution among all three stacks can be achieved without having to operate the device at very high bias voltage.

Figure 7 shows the dark current density-voltage (J-V) characteristics measured at different temperatures for the 3 stacks along with the 300K- background window current density with a 180° field of view (FOV). Figure 7 (a) shows the dark J-V curves for the bottom stack measured at T = 40, 60, 77, 90K. The device is under background limited performance (BLIP) for $-2.8V < V_b < 0V$, at T = 60K. Figure 7 (b) shows the dark J-V curves for the middle stack measured at T= 40, 60, 77 and 90K, and the BLIP condition occurs at V_b= -0.5V, T= 77K and at V_b= 1.1V, T = 90K. Figure 7 (c) shows the dark J-V curves for the top stack measured at T= 30, 40, 50, 60, 77 K, and the device is under BLIP condition over the entire range of the applied bias, at T = 30K. The MWIR stack, with the highest effective barrier height, has the lowest dark current density under same temperature and bias conditions as the LWIR and VLWIR stacks. The asymmetrical dark current versus bias characteristic observed in the bottom and top stacks is attributed to the asymmetrical barrier height under the positive and negative bias conditions. This asymmetrical behavior is more obvious in the bottom stack due to the steeper slope of the graded barrier. However, the asymmetrical dark J-V curves observed in the middle stack

were caused by the dopant impurity migration effect associated with the MBE growth. The photocurrent spectra were measured with a 45° facet backside illumination using a

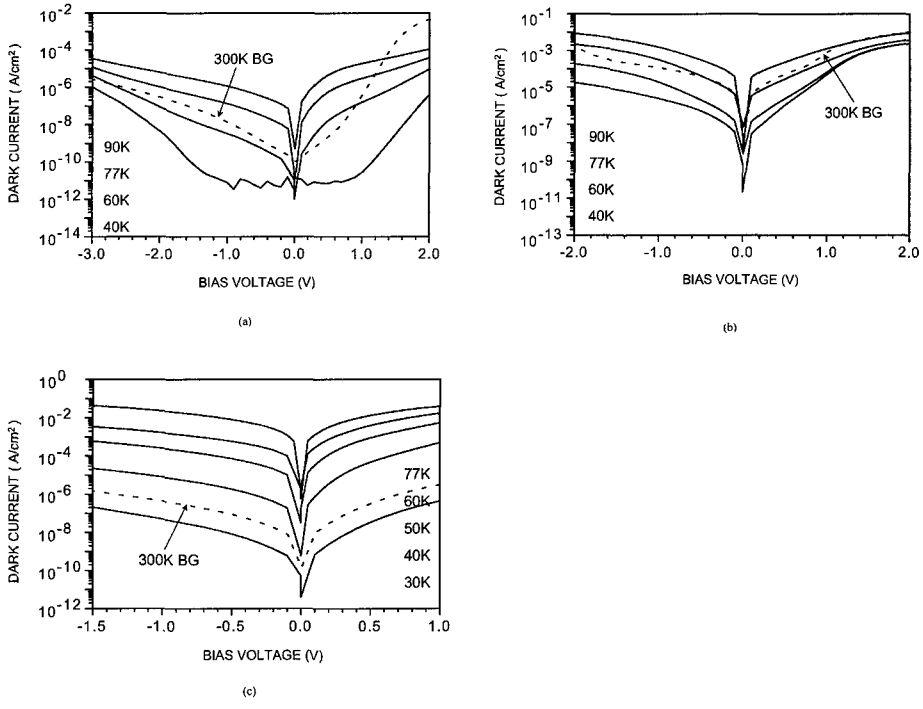

Figure 7 Dark J-V characteristics of the 3-stack 3-color QWIP: (a) MWIR stack; (b) LWIR stack, and (c) VLWIR stack.

calibrated blackbody source at 1000 K. Figure 8 (a) shows the spectral responsivity of the bottom stack measured at 40K for the MWIR stack. The peak detection wavelength is λ_p = 6.5 μm, which agrees well with the calculated value, and was found nearly independent of temperature and applied bias voltage. The cut-on and cut-off wavelengths for the full-width at half- maximum (FWHM) are 5.9 μm and 7.0 μm, respectively, with $\Delta \lambda/\lambda_p$= 16.9%. The detection bandwidth for this stack covers the major portion of the water- blocking band. A peak responsivity of 0.13 A/W at λ_p = 6.5 μm was obtained at V_b = -0.13V and T = 40K, and it remains nearly constant for temperatures up to 77K. A dark-current detectivity of $D^* = 8.5\times10^{12}$ cm-Hz$^{1/2}$/W at V_b= -1.3V, T= 40K was obtained for this stack.

Figure 8 (b) shows the spectral responsivity measured at different biases for the middle stack at T = 40K. The peak detection wavelength is at λ_p = 10.1 μm for this stack. The result shows a slight red- shift compared to the calculated peak wavelength, which may be attributed to the uncertainty of the conduction band offset value used in our calculation. The FWHM for this middle stack is 9.1 μm ~11.2 μm, with $\Delta \lambda_p$= 20.8%, which covers the entire ozone band. A peak responsivity of 1.08 A/W was obtained at λ_p = 10.1 μm, V_b = -1.4V and T = 40K, with a detectivity of D^* = 1.5×10^{10} cm-$Hz^{1/2}$/W.

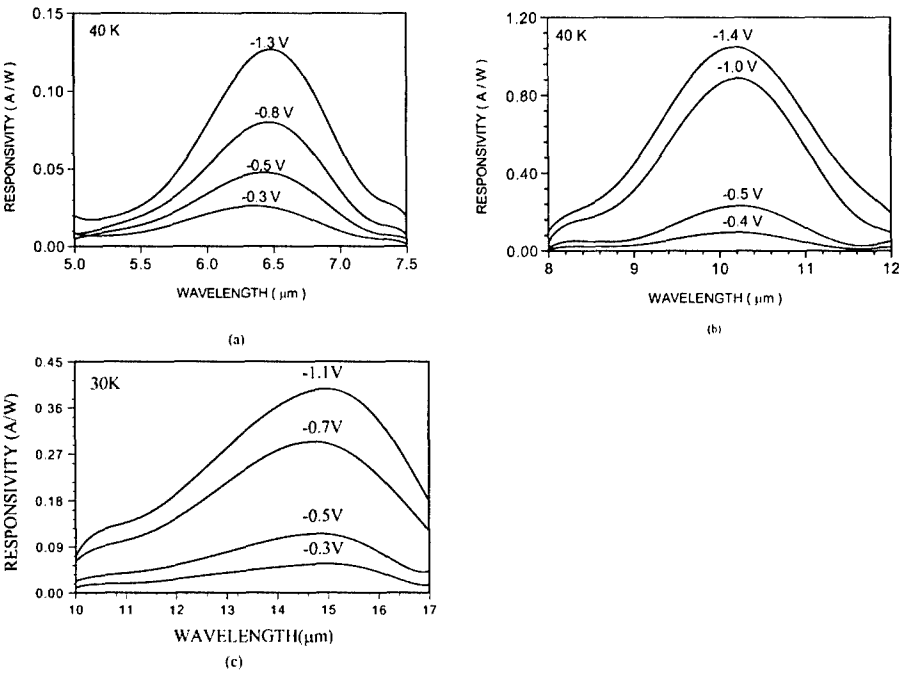

Figure 8 Spectral responsivity of the 3-stack 3-color QWIP for MW/LW/VLWIR detection: (a) MWIR stack, (b) LWIR stack, and (c) VLWIR stack.

Figure 8 (c) shows the spectral responsivity of the top stack measured at T = 30 K. The peak detection wavelength is at 15.1 μm for this VLWIR stack. The FWHM is from 12.2 μm to 16.9 μm with $\Delta \lambda_p$=31.1%, which covers the CO_2 band. The peak responsivity is 0.42 A/W at λ_p = 15.1 μm, V_b = -1.1V and T = 30 K, with D^* = 1.2×10^{11} cm-$Hz^{1/2}$/W. The value of D^* decreases sharply with increasing temperature to 8.3×10^9 cm-$Hz^{1/2}$/W at V_b=-0.2V, λ_p=15.1μm, and T = 40K. Reported D^* values for the VLWIR (λ_p=15~17.5 μm) InGaAs/AlGaAs QWIPs were in the 10^9 ~10^{12} cm-$Hz^{1/2}$/W range for T= 20K~ 40K. [21-24] It should be pointed out that the H_2O and CO_2 bands are not

completely blocked in the atmosphere. Thus, the optical signals are not totally blocked in the atmosphere, and the ozone layer does not influence the optical signal measuring on the earth surface. As a result, a relatively large spectral responsivity can still be obtained in this 3- stack 3- color QWIP.

In summary, we have demonstrated a high performance 3-stack 3-color QWIP designed specifically for the exo- atmospheric detection with peak detection wavelength centered at the water, ozone, and CO_2 blocking bands in the atmosphere. The characteristic and performance of this 3-stack 3-color QWIP have been depicted in this section. The detection bandwidths of this QWIP over the majority or entire region of the three blocking bands in the atmosphere, and the detector can be used for the exo-atmospheric multi-color IR FPAs imaging applications.

4. CONCLUSIONS

In this paper, the design, growth, and characterization of a 2-stack 3-color QWIP for MW/LW/LW IR detection and a 3-stack 3-color QWIP for MW/LW/VLW IR detection have been depicted. Excellent performance in both QWIPs has been achieved. The flexibility of the QWIP structures by the MBE growth made the QWIP device an excellent candidate for multi-color FPAs applications in the MWIR to VLWIR spectral windows.

ACKNOWLEDGEMENT

This work was supported in part by the US Army Research Office under contract No.DAAD19-01-1-0673. The author would like to thank Dr. Bill Clark for his interest and support in this work. He would also like to thank Dr. Meimei Tidrow of BMDO for her continued support of the QWIP research at UF. The author would also like to acknowledge the contributions of Ling Jiang and Jung-Hee Moon for the characterization of QWIP devices reported in this paper.

REFERENCES

1. R. B. Emmons, S. R. Hawkins, and K. F. Cuff, Opt. Eng. **14**, 21 (1975).

2. L. Serzhenko and V. D. Shadrin, Sov. Phys. Semicond. 25, 953 (1991).

3. L. L. Chang, L. Esaki, and G. A. Sai-Halaz, IBM Tech. Discl. Bull. **20**, 2019 (1977).

4. L. Esaki and T. Tsu, IBMJ. Res. Develop. **14**, 61 (1970).

5. L. Esaki and H. Sakaki, IBM Tech. Discl. Bull. **20**, 2456 (1977).

6. D. D. Coon and R. P. G. Karunasiri, Appl. Phys. Lett. **45**, 649 (1984).

7. L. C. West and S. J. Eglash, Appl. Phys. Lett. **46**, 1156 (1985).

8. A. Harwit and J. S. Harris, Jr., Appl. Phys. Lett. **50**, 685 (1987).

9. B. F. Levine, K. K. Choi, C. G. Bethea, J. Walker, and R. J. Malik, Appl. Phys. Lett. **50**, 1092 (1987).

10. B. F. Levine, C. G. Bethea, G. Hasnain, V. O. Shen, E. Pelve, R. R. AB-Bot, and S. J. Hsieh, Appl. Phys. Lett. **56**, 851 (1990).

11. L. S. Yu and S. S. Li, Appl. Phys. Lett. **59**, 1332 (1991).

12. B. F. Levine, J. Appl. Phys. **74**, R1 (1993).

13. I. Gravé, A. Shakouri, N. Kuze, and A. Yariv, Appl. Phys. Lett. **60**, 2362 (1992).

14. Sheng S. Li and M. Z. Tidrow, "Quantum Well Infrared Photodetectors," Handbook of Nanostructured Materials and Nanotechnology, edited by H. S. Nalwa, **vol.4**, chapter 9, pp.561-619, Academic Press, Oct., 1999.

15. J. C. Chiang, Sheng S. Li, M. Z. Tidrow, P. Ho, M. Tsai, and C. P. Lee, Appl. Phys. Lett., vol. 69, pp. 2412-2414, Oct. 1996.

16. Xudong Jiang, Sheng S. Li, and M. Z. Tidrow, IEEE J. of Quantum Electronics, vol. 35, pp. 1685-1692, Nov. 1999.

17. J. C. Chiang, Sheng S. Li, and A. Singh, Appl. Phys. Lett., vol. 71, pp. 3546-3548, Dec. 1997.

18. W. R. Dyer, Electrochemical Society Proceedings Vol. 99-22, 425(1999).

19. A. K. Ghatak, K. Thyagarajan and M. R. Shenoy, IEEE J. Quantum Electronics, **24**, 1524 (1988).

20. H. C. Liu, J. Appl. Phys. 73, 3062 (1993).

21. G.Sarusi, S.D. Gunapala, J.S. Park and B.F. Levine, J. Appl. Phys., 76, 6001 (1994).

22. B.F.Levine, A.Zussman, J.M.Kuo and J. De Jong, J.Appl. Phys, 71, 5130 (1992).

23. S.D. Gunapala, K.M.S.V. Bandara, B.F.Levine, G. Sarusi, D.L. Sivco and A.Y. Cho, Appl. Phys. Lett. , 64, 2288 (1994).

24. C.Y. Lee, M.Z. Tidrow, K.K. Choi, W.H. Chang, L.F.Eastman, F.J. Towner and J.S.Ahearn, J. Appl. Phys., 75, 4731 (1994).